Journal of Biomedical Optics

BiomedicalOptics.SPIEDigitalLibrary.org

Wide-field imaging of retinal vasculature using optical coherence tomography-based microangiography provided by motion tracking

Qinqin Zhang
Yanping Huang
Thomas Zhang
Sophie Kubach
Lin An
Michal Laron
Utkarsh Sharma
Ruikang K. Wang

SPIE.

Wide-field imaging of retinal vasculature using optical coherence tomography-based microangiography provided by motion tracking

Qinqin Zhang,[a] Yanping Huang,[a] Thomas Zhang,[b] Sophie Kubach,[b] Lin An,[b] Michal Laron,[b] Utkarsh Sharma,[b] and Ruikang K. Wang[a,*]
[a]University of Washington, Department of Bioengineering, 3720 NE 15th Avenue, Seattle, Washington 98195, United States
[b]Carl Zeiss Meditec, Inc., 5160 Hacienda Drive, Dublin, California 94568, United States

Abstract. Optical coherence tomography (OCT)-based optical microangiography (OMAG) is a high-resolution, noninvasive imaging technique capable of providing three-dimensional *in vivo* blood flow visualization within microcirculatory tissue beds in the eye. Although the technique has demonstrated early clinical utility by imaging diseased eyes, its limited field of view (FOV) and the sensitivity to eye motion remain the two biggest challenges for the widespread clinical use of the technology. Here, we report the results of retinal OMAG imaging obtained from a Zeiss Cirrus 5000 spectral domain OCT system with motion tracking capability achieved by a line scan ophthalmoscope (LSO). The tracking LSO is able to guide the OCT scanning, which minimizes the effect of eye motion in the final results. We show that the tracking can effectively correct the motion artifacts and remove the discontinuities and distortions of vascular appearance due to microsaccade, leading to almost motion-free OMAG angiograms with good repeatability and reliability. Due to the robustness of the tracking LSO, we also show the montage scan protocol to provide unprecedented wide field retinal OMAG angiograms. We experimentally demonstrate a 12×16 mm^2 retinal OMAG angiogram acquired from a volunteer, which is the widest FOV retinal vasculature imaging up to now in the community. [DOI: 10.1117/1.JBO.20.6.066008]

Keywords: optical coherence tomography; optical microangiography; wide field imaging; motion tracking; retinal microcirculation.
Paper 140770R received Nov. 20, 2014; accepted for publication May 28, 2015; published online Jun. 23, 2015.

1 Introduction

Ophthalmic imaging has emerged as one of the most successful applications for optical coherence tomography (OCT) since its invention in the early 1990s.[1] The capability of OCT to provide noninvasive, noncontact, high-resolution, high-sensitive, and depth-resolved imaging of microstructures in the retina and eye has been a key factor for its success.[2] Without a doubt, OCT has proved to be a disruptive technology in ophthalmology as it can provide unprecedented clinically useful information to aid the diagnosis and treatment of eye diseases. Over the last decade and a half, commercial ophthalmic OCT technology has advanced rapidly with continued improvements in the hardware, ease of use, and OCT data analysis features to aid in diagnostics or management of the progression of diseases.[3] Spectral domain OCT (SD-OCT)[4,5] has been rapidly adopted and gained wide spread use in ophthalmic imaging applications, including both clinical and research. The increased imaging speed and sensitivity of SD-OCT over time-domain OCT has produced its accelerated impact on retinal imaging. In contrast to the currently available clinical imaging techniques such as fluorescein angiography (FA) and indocyanine green angiography (ICGA), OCT provides a noninvasive approach to rapidly assess three-dimensional (3-D) high-resolution microstructural information of the retina. While the clinical use of OCT has increased tremendously over the past decade, the use of traditional imaging strategies such as FA and fundus photograph have commensurately declined.

However, the traditional OCT technique is based on structural imaging, which gives limited functional information about the retina. OCT angiography, for example, optical microangiography (OMAG),[6,7] has recently generated increasing interest in the OCT and ophthalmic research community. OMAG-based OCT angiography is one of the leading techniques that is capable of providing the distribution of functional blood vessels including capillaries within tissue beds *in vivo*.[6,7] This measurement is less sensitive to the Doppler angle as experienced in Doppler-based flow measurement.[8] OMAG has been applied to visualize high-resolution and high-contrast mapping of capillary networks in the retina and choroid.[9,10] OMAG has demonstrated clinical utility by imaging a range of retinal diseases including diabetic retinopathy and macular telangiectasia and drawing useful comparisons of imaging performances when compared with FA images.[11,12] FA and ICGA still remain the gold standards for diagnosis of any vasculature abnormality in the eye. However, the invasiveness of the dye injection combined with possible adverse reactions to the dye, such as nausea or anaphylactic response in some rare cases, makes it an unsuitable technique for frequent and widespread ophthalmic screening applications. Hence, the attractiveness of using OMAG for vascular pathologies in the eye is further emphasized as it is a noninvasive imaging technique. In addition, OMAG provides

*Address all correspondence to: Ruikang K. Wang, E-mail: wangrk@uw.edu

high-resolution depth sectioning capability for high-resolution microvascular visualization of the eye.

Although OMAG has demonstrated early clinical utility by imaging diseased eyes, it needs to overcome several technical challenges to be able to consistently provide useful, artifact-free and repeatable imaging performance. The two biggest challenges for the widespread clinical use of the technology are the limited field of view (FOV) imaging capability and the sensitivity to eye motion artifacts. OMAG requires dense sampling and repeated measurements over the same location in the eye that can limit the area being scanned for a given acquisition time, thereby reducing the imaging FOV.

The human eye is in constant motion that is caused by involuntary fixational eye movements, e.g., microsaccades and drift.[13] This eye motion currently remains a major challenge for OMAG to provide the images of functional retinal microvasculature with high fidelity, because the motion would inevitably result in motion artifacts in the final results. To mitigate this eye motion problem, one obvious approach is to increase the imaging speed of the OCT systems. However, it is not often practical for commercial OCT systems because the fastest food and drug administration approved OCT system so far is of ~100 kHz implemented by swept-source configuration, e.g., Atlantis swept source OCT (Topcon Inc., Japan); and for SD-OCT, this speed is lowered to 70 kHz, e.g., Cirrus HD-OCT (Carl Zeiss Meditec Inc.). Even when the scanning speed is fast enough, the motion artifacts are still present in the OCT anatomical images,[14,15] thereby affecting the interpretation and the quantitation of OMAG retinal microvascular images. Postprocessing methods are also developed to remove the eye motions,[16,17] but they do not work well for large and rapid eye movement, resulting in difficulty in the visualization and quantification of volumetric images.

Another method to eliminate eye motion artifacts is to monitor eye motion and correct the imaging system in real-time, namely an eye-tracking system. As discussed in Refs. 18 and 19, several approaches have been proposed to track and quantify eye motion. These methods include the measurement of the anterior segment movement by the use of magnetic search coils,[20] the monitoring of certain reflections from anterior optics,[21,22] or the tracking of reflections from tightly fitted contact lenses with tiny mirrors.[23] Another tracking method utilizes the retinal image to provide the lateral motion of a blood vessel with a line-scan camera,[24] a precursor to a current scanning laser ophthalmoscope (SLO).[25,26] An SLO-based method was described for tracking retinal motion by the frame rate[27] and analyzing distortions within sections of individual frames.[28,29] Currently, commercial OCT instruments have implemented eye tracking in the system so that eye motion can be measured and corrected in real-time, e.g., Cirrus HD-OCT (Carl Zeiss Meditec Inc.), Spectralis OCT (Heidelberg Engineering, Heidelberg, Germany), RTVue (Optovue Inc., California), and tracking OCT from Physical Sciences Inc. (PSI).[30,31] All of these systems use the measured eye motion signal to control the OCT scanning grid on its moving retinal target using either the OCT galvanometer scanners or secondary tracking scanners. In terms of angiography or blood flow imaging, the PSI tracking technology was reported for stabilizing SLO-based laser Doppler flowmetry[32] and FA/ICGA imaging.[33] Up to now, the eye tracking has only been used for OCT-structural imaging purposes in the commercial systems. There is only one academic report that described an optical frequency domain imaging system combined with experimental real-time tracking SLO to correct the eye motion[18] to provide phase-resolved OCT angiography.[19]

In this paper, we present OMAG retinal microvascular results by leveraging the motion tracking capability available in the commercial CIRRUS HD-OCT 5000 from Carl Zeiss Meditec Inc. The Cirrus HD-OCT is equipped with a proprietary motion tracking mechanism achieved by an auxiliary real time line scan ophthalmoscope (LSO). OMAG scanning protocol was implemented in the system to provide almost motion-free retinal vascular imaging *in vivo*. Furthermore, we show that the eye tracking system enables montaging of multiple cube scans to create a large FOV vascular image without eye motion artifacts on healthy volunteers.

2 Experimental System, Test Procedure, and Data Processing

The OMAG scanning protocol was implemented in a CIRRUS HD-OCT 5000 (Carl Zeiss Meditec Inc. Dublin, California) system that operates on a central wavelength of 840 nm and an A-scan speed of 68,000 A-scans/s. The bandwidth of the light source is 45 nm, giving an axial resolution of ~5 μm in tissue. The lateral resolution is ~15 μm. The combined optical power on the cornea from OCT and SLO light sources was measured to be less than 0.8 mW, which is within the American National Standards Institute standards for laser safety. During imaging, measures were taken to minimize possible head movements of the subject. Before OCT data acquisition, the subject was asked to place his/her head on a chin-cup with forehead leaning in contact with a forehead rest. A fixation point in the center of the view was used as the target for the subject to minimize saccades of eye during scanning. The basic procedures for an eye scan are: the head is first placed in the chin-cup; the distance between the eye and the OCT scanner is adjusted for a better view of the iris image for localization; then auto-focus is performed to focus the OCT probe beam on the retina; after that, a scan region of interest is selected and the OCT signal is optimized through autofocus, reference mirror position adjustment, and polarization control; and finally, 3-D volume OCT data are acquired and saved for offline processing and analyses.

To achieve OMAG imaging of retinal vasculatures, a repeated B-mode scan protocol was adopted to acquire volumetric datasets, i.e., a number of repeated B-scans were acquired at each spatial step over the slow axis direction (y-axis).[34] For each B-scan, the number of A-scans was 240, covering a lateral distance of ~2.4 mm. The direction of the B-scan is called the fast scan direction (x). In the slow scan direction, the scan was stepped (200 steps) through a range of 2.4 mm. We define cluster scan as the number of repeated B-scans at the same location, hence, each step in the slow axis represents a cluster scan. In each step, B-scans were repeated four times in the current study for extracting the flow signal because this number has been tested to provide a reasonable imaging performance for OMAG in terms of acceptable imaging time and image quality.[10,34] The time difference between two successive B-scans was ~4.5 ms, roughly corresponding to a frame rate of 224 fps. Based on this scan protocol and system speed, the total time for a single volume acquisition was about 3.6 s, not including the adjustment time before the data collection. However, when there is severe motion in subject, the time of a single volume acquisition would be increased due to motion tracking. The system, however,

would automatically stop the scanning if the acquisition time for a single volume reaches 7 s.

The use of Cirrus 5000 HD-OCT OMAG prototype for *in vivo* measurements in humans was approved by the Institutional Review Board of the University of Washington. Informed consent was obtained from each volunteer subject before imaging. All procedures adhered to the tenets of the Declaration of Helsinki.

2.1 *Motion Tracking Line Scan Ophthalmoscope*

To reduce/minimize the motion artifacts in the final OMAG/OCT images, a proprietary motion tracking system using an LSO was used to guide OCT-scans.[35] This motion tracking capability is already available in the commercial Cirrus HD-OCT 5000 system for OCT anatomical imaging (for details see Ref. 36). Very briefly, the initial LSO frame is first selected as a reference. The subsequent LSO frames are used to correlate with the reference frame, from which the eye motion signals, and thus eye fixation shift information was derived. The fixation shift information is used to modify the waveforms that drive the OCT galvanometer scanners to collect scans at the right location. Additionally, the tracking LSO drives the SD-OCT with a validity signal in case of tracking failures. Subthreshold correlation of the current frame with the reference frame is defined as tracking failure.[18] Low correlation is possible when there is large drift, large saccade, vertical motion, blink or misalignments of the pupil. If this is the case, it is considered as an invalid signal. If an invalid signal is received, the SD-OCT discards the invalid scans and reacquires them.

2.2 *Data Processing*

After the 3-D volume dataset is acquired, an OMAG algorithm is applied to extract blood flow information.[6,7,34,37] The algorithm is based on an OCT-complex signal differentiation approach that was recently published.[6,7] In brief, the OCT signals between adjacent B-scans are directly differentiated among the 4-repeated B-scans, and then averaged to achieve one cross-sectional blood flow image. After the B-scans at all steps in the slow scan direction are processed, the 3-D OMAG image is generated, representing the retinal vasculature map within the scanned tissue volume. Meanwhile, the residual displacement occurring between adjacent B-scans due to involuntary eye movement is compensated for by two-dimensional (2-D) cross correlation between two adjacent OMAG flow images.[38,37]

2.3 *Segmentation and Definition of Retinal Layers*

A semiautomated retinal layer segmentation algorithm recently published in Ref. [39] was used to segment different layers from the OCT cross-sectional structural images based on intensity differences. Briefly, the segmentation is based on the automatic detection of the highest magnitude gradient in OCT intensity B-scans for specific tissue interfaces. When it is difficult to find the correct interface, the operator can interrupt the automatic algorithm and manually find the correct interfaces. Segmentation is conducted on the entire 3-D data volume. The positions of each interface are saved after tracing of the entire 3-D data is completed, from which physiological retinal layers are identified. The segmentation results are equally applicable to both the OCT structure images and the OMAG vascular images to produce the enface images of either microstructure or vasculature. The enface image of each layer can be generated by 2-D maximum projection of either OCT or OMAG signals. In the retina, three layers are segmented for normal subjects to represent the vascular networks at different depths, which include nerve fiber layer (NFL), inner retinal layer (including ganglion cell layer and inner plexiform layer), outer retinal layer (including inner nuclear layer and outer plexiform layer). The overlay angiograms are also produced and coded with different colors to give a distinct vasculature network at different depths. The segmentation would help us investigate the vascular changes in different layers, useful for identifying the early stages of diseases.

3 Results and Discussions

In this section, we demonstrate the results of eye tracking for OMAG. First, the tracking performance was tested on an eye phantom model. Then healthy volunteers were recruited and their eyes were imaged using two imaging modes, i.e., with and without motion tracking in the system. This illustrated the distortions and artifacts caused by microsaccades and drift, and their effective corrections by motion tracking in final retinal OMAG angiograms. Finally, we showed that the tracking feature in the OCT system enabled the ultrawide view imaging of retinal vasculature, ~67 degrees of view, which is the widest FOV functional imaging capability demonstrated in the OCT community.

3.1 *Tracking Performance in the Eye Phantom*

To test the performance of tracking LSO, we first used an eye phantom model (Carl Zeiss Meditec Inc. Dublin, California) to demonstrate the motion correction in the tracking system before imaging a human eye. The model eye was placed steadily in the sample arm. A square area of the macular was imaged, including 240 A-lines and 200 B-scans covering ~2.4×2.4 mm^2. Following the experimental procedure as described in Refs. 18 and19, three conditions were tested and the resulting enface images were generated. The three conditions included: (1) no-motion without tracking; (2) motion without tracking, and (3) motion with tracking. The motion was induced by lightly tapping on the phantom eye randomly during imaging. Figure 1 shows the results under the three conditions. Figure 1(a) shows the model eye imaged without motion in the retina and the tracking system turned off. The motion artifacts induced randomly in the model eye were imaged with the tracking off as shown in Fig. 1(b), where the distortion is obvious. The result under the 3rd condition [Fig. 1(c)] shows how tracking corrects the motion when the motion was introduced into the system. From the comparison between Figs. 1(a) and 1(c), the original structure image is recovered when the tracking system is enabled, demonstrating the efficiency of motion tracking to deliver undistorted OCT images.

3.2 *Tracking Performance in Human Eye*

Previous reports have shown that the eye motion can create severe artifacts and induce discontinuities and distortions of blood vessels.[40,41] Tracking improves the ability to make repeatable measurements based on OCT structural information. For example, Hu et al.[42] had demonstrated improved repeatability of retinal thickness measurements using a Zeiss Cirrus HD-OCT LSO-based tracking system. Without motion tracking, Figs. 2(a) and 2(b) demonstrate the OMAG angiogram of the

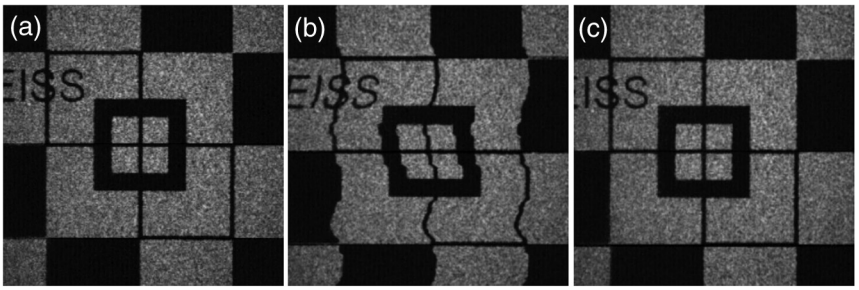

Fig. 1 Enface optical coherence tomography images of the model eye under three conditions: (a) no motion is introduced and tracking system disabled, (b) motion is introduced randomly but tracking is turned off, and (c) motion is the same as in (b) but tracking is enabled to compensate motion. The original structure image of model eye is totally recovered when the tracking is on. The image size is 2.4×2.4 mm^2.

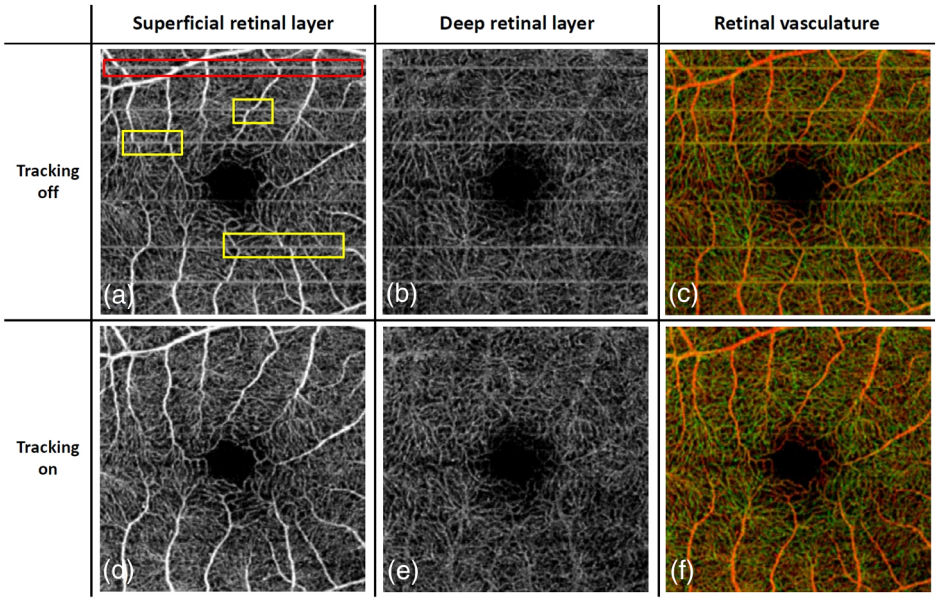

Fig. 2 Enface retinal vasculatures obtained by optical microangiography (OMAG) under the conditions of without tracking (top) and with tracking (bottom): (a) and (b) the enface angiograms of inner and outer retinal layers with the artifacts of horizontal strips (arrows) and the vessel discontinuities of vessel (boxes), (c) the false color enface vascular map after merging (a) with (b), (d)–(f) corresponding enface angiograms with the motion tracking enabled. The tracking system works well in eliminating the motion-caused artifacts. The red color in (c) and (f) indicates the inner retinal layer, and the green color the outer retinal layer. The image size is 2.4×2.4 mm^2.

inner and outer retinal vasculature in the macula region (fovea) of a healthy volunteer, where motion artifacts are obvious. The white horizontal line artifacts in the angiograms are generated by the microsaccades [highlighted by arrows as examples in Fig. 2(a)]. This is because the eye movement causes the adjacent B-scans to not be acquired at the exact same location, leading to decorrelation among the repeated B-scans at that location. Further, these motion artifacts are responsible for the discontinuities of blood vessels in the angiogram [highlighted by boxes in Fig. 2(a)]. Depending on the direction of the microsaccades, these discontinuities often give rise to a repetition, or loss, of a certain blood vessel (or a group of vessels). However, it is difficult to identify the drift caused by the positional changes of the eye from individual angiograms. The eye drift causes a slow variation in position over time, which leads to displacements in the angiogram and affects the accuracy of the spatial position of the vasculature. It is necessary to correct the drifts to provide more precise vasculature distribution. The color-coded enface angiogram in Fig. 2(c) is the whole retinal vasculature under the nontracking condition, in which the red indicates the inner retinal layer and the green the outer retinal layer. The connections of vessels between the inner and outer retinal layers are hard to observe due to the artifacts. The foveal avascular zone (FAZ) is also affected by the artifacts [Fig. 2(c)], which would impact our ability to accurately quantify the FAZ area.

The resulting enface retinal angiograms, when the motion tracking feature in the system was enabled, are shown in Figs. 2(d)–2(f), respectively. It can be seen that the artifacts caused by microsaccades, e.g., the white lines and vessel discontinuities, are effectively corrected, giving a smooth and precise FAZ. Meanwhile, the vascular connections of different layers are observed in Fig. 2(f).

The clear and artifact-free angiograms would be important to provide precise vascular information to aid in the diagnosis and

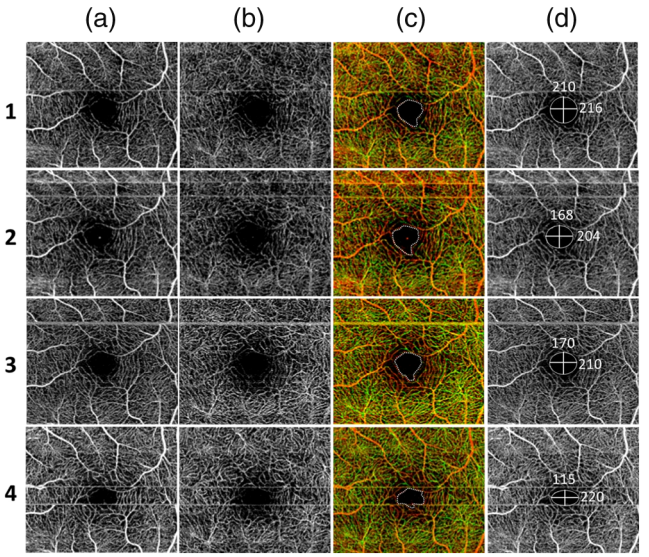

Fig. 3 Reliability of retinal vasculatures obtained by OMAG without tracking. The results were obtained from the same subject at four different time intervals. Shown from left to right are the enface angiograms of (a) inner retina, (b) outer retina, (c) depth-color encoded enface whole retina, and (d) maximum intensity projection of whole retina, respectively. In the color images, the red color indicates the inner retinal layer; and the green color the outer retinal layer. The image size is 2.4×2.4 mm^2.

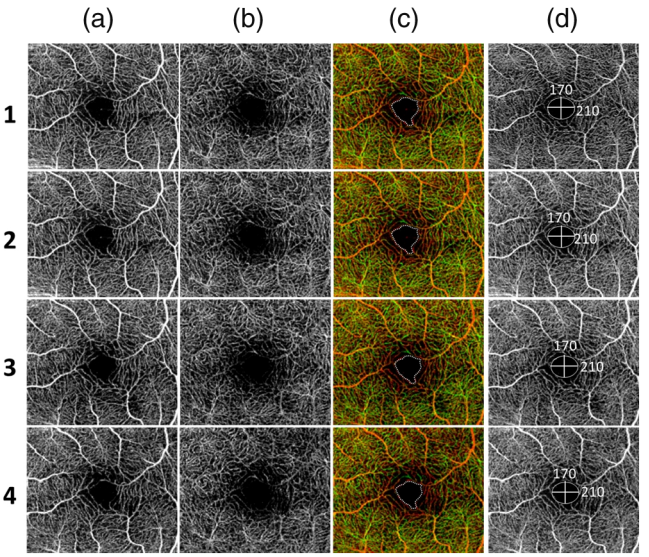

Fig. 4 Reliability of retinal vasculatures obtained by OMAG with tracking. The results were obtained from the same subject as in Fig. 3 at four different time intervals. Shown from left to right are the enface angiograms of (a) inner retina, (b) outer retina, (c) depth-color encoded enface whole retina, and (d) maximum intensity projection of whole retina, respectively. In the color images, the red color indicates the inner retinal layer, and the green color the outer retinal layer. The image size is 2.4×2.4 mm^2.

treatment of retinal diseases. For example, in the assessment of the progression as well as the therapeutic treatment of diabetic retinopathy, one of the important clinical parameters is to evaluate the variations of FAZ over time. In this regard, the system must provide reliable and undistorted macular vascular maps every time when the patient visits the clinic. This requirement can be fulfilled with the motion-tracking OCT-based microangiography described herein.

To show the usefulness of the motion tracking to provide reliable measurement of FAZ, experiments were conducted to collect the OMAG image over the fovea multiple times. In the experiment, the subject was imaged four times, of which three scans were performed approximately 2 h apart, and one more scan was collected the next day. In each scan session, two OMAG images were collected: one with and another without motion tracking enabled. The results are shown in Fig. 3 without tracking and in Fig. 4 with tracking enabled, respectively, where it is clear that the imaging without motion tracking gives distorted images from one scan to another, leading to difficulty in the interpretation of the vascular images, and more importantly inaccurate measurement of the FAZ over time. However, with motion tracking enabled, the OMAG images were quite repeatable, providing almost identical vascular appearance and connectivity. From the images, we also quantified the FAZ. In the quantification, we first manually drew the contour line that encloses the FAZ (see the dashed line in the false-color images), upon which an ellipse (shown in the right column of Figs. 3 and 4) was fitted by the use of least square fitting algorithm to provide the long (horizontal) and short (vertical) axis lengths. In addition, we also provided the measurements of the FAZ area upon each visit, defined by the enclosure of the manually drawn contour line. The results are provided in Figs. 3 and 4, respectively, and are also tabulated in the Table 1, demonstrating the excellent repeatability and reliability of the FAZ measurements over time by the use of motion tracking features in the system. However, it must be noted that this study is not meant to provide a meaningful comparative performance of tracking versus untracked data acquisition as only a single subject was imaged. Rather, the focus has been to demonstrate that the benefits of tracking-based OCT acquisition could be extended to its functional extension of OCT angiography.

3.3 *Ultrawide-Field Retinal Imaging Based on Tracking Line Scan Ophthalmoscope*

Wide-field OCT angiography visualization has been generated previously by mosaicking multiple volume acquisitions.[43,38] However, due to lack of tracking, the prior approaches involved complex postprocessing steps such as splitting a vasculature enface image into segments of artifact free bands and using an acquisition scheme that requires two acquisitions over the same area with orthogonal fast axis scans. In addition to the complexity in postprocessing, this method may not work well enough in situations where the subject is not able to refixate at the same location after the involuntary motion. In our approach, we address these challenges by the use of LSO-based tracking that makes it feasible to acquire a large FOV of retinal vasculature. To achieve this, a montage scanning protocol was implemented under the motion tracking mode to acquire multiple cube scans. In this protocol, the multiple cube scans proceeded one after another at predefined locations (grid) on the retina. There was 10% overlap between adjacent cubes, providing enough space to stitch the images together and avoiding the missing information after all the grids were scanned. It is important to note that during the montage scanning, subjects are not restricted to maintain fixation or to not blink during the entire acquisition. They can have a rest in between scans, and then place their head back onto the chin-rest again for the next scan.

Table 1 Quantitative assessment of foveal avascular zone against multiple scans.

Tracking mode	Measurement	1	2	3	4	Average
OFF	Long axis (μm)	216	204	210	220	212.5 ± 7
	Short axis (μm)	210	168	170	115	165.8 ± 39
	Contour area (mm^2)	0.114	0.127	0.118	0.090	0.112 ± 0.016
ON	Long axis (μm)	210	210	210	210	210 ± 0
	Short axis (μm)	170	170	170	170	170 ± 0
	Contour area (mm^2)	0.119	0.120	0.116	0.117	0.118 ± 0.002

The tracking LSO will automatically correct for eye motion for the next cube scan. In the current study, the maximum scanning region for one montage scan is set to 6×7 grids (or 42 cube scans in total), covering approximately 12×16 mm^2 on the retina (roughly 67 degrees of view).

For demonstration, a female volunteer (28 years old) was imaged by the use of the montage protocol. After all 42 cube scans were collected, postprocessing was completed to obtain the retinal vascular images for all the cubes, which were then stitched together to form a large FOV image. Three layers

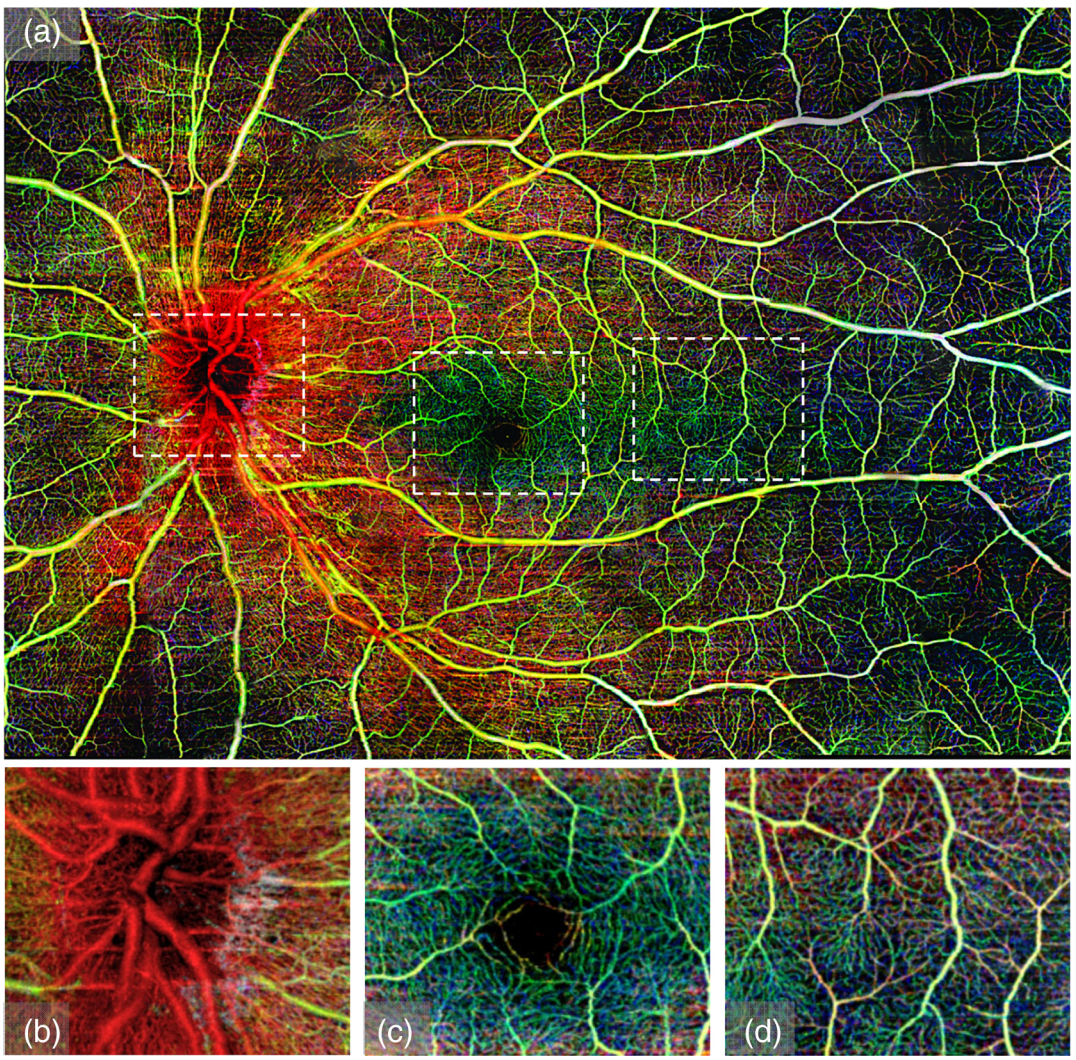

Fig. 5 (a) Wide field retinal vasculature of a healthy volunteer coded with different colors according to three layers obtained by montage scanning protocol of OMAG, (b)–(d) the magnified OMAG angiograms corresponding to the white rectangles in (a) to demonstrate the detail of blood vessel in different region, including (b) optic nerve head, (c) fovea, and (d) temporal region. The size of (a) is 12×16 mm^2. The size of (b)–(d) is 2.0×2.4 mm^2.

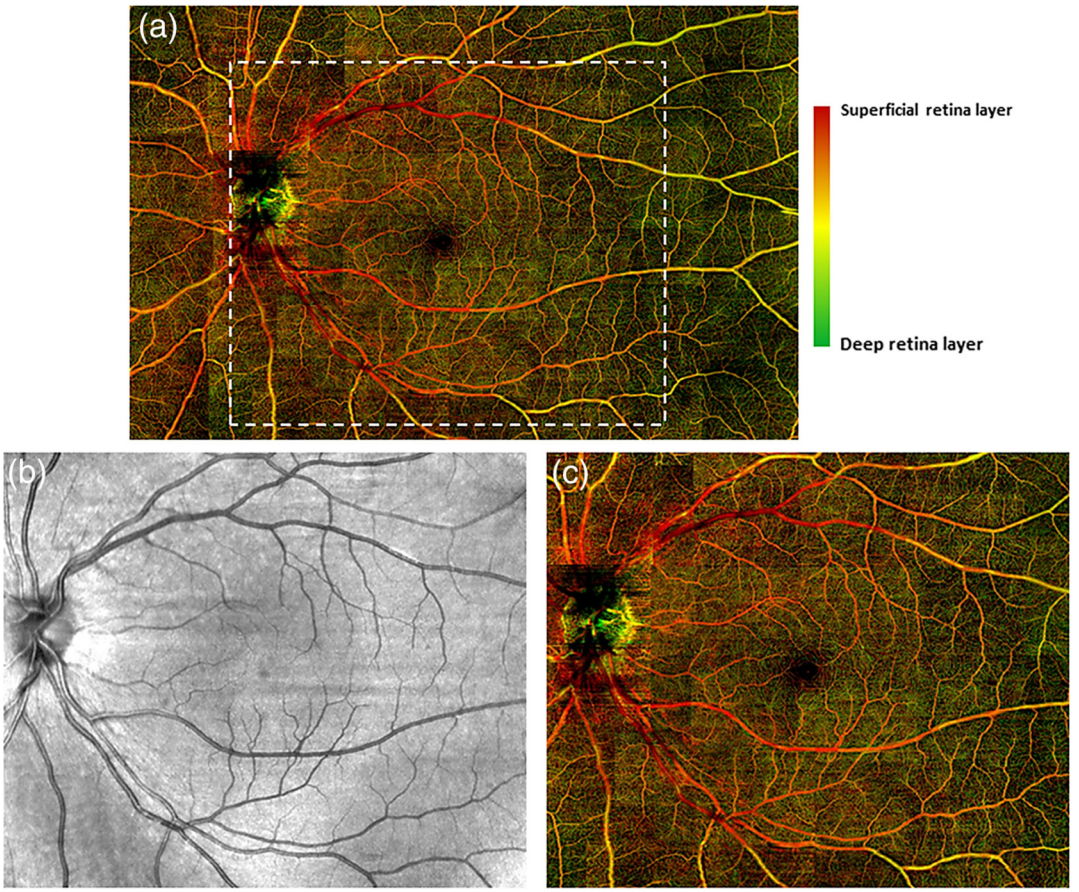

Fig. 6 (a) Wide field retinal vasculature of a healthy volunteer coded with different colors according to two layers [excluding nerve fiber layer (NFL)] obtained by montage scanning protocol of OMAG. Excluding the NFL, the details of retinal vessels can be more appreciated. For comparison, (b) the scanning laser ophthalmoscope (SLO) image, and (c) the corresponding OMAG angiograms. A much better visualization of vascular tree is observed when compared to SLO image. The size of (a) is 12×16 mm^2. The size of (b) and (c) is 11×9 mm^2.

(described in Sec. 2.3) were segmented to give a better demonstration of retinal vasculature according to depth. Figure 5(a) shows the results of the wide field OMAG angiogram ($\sim 12 \times 16$ mm^2), which includes NFL, inner retinal layer, and outer retinal layer. The color-coded information is as follows: red represents NFL, green represents inner retinal layer, and blue is outer retinal layer. The tracking LSO provided a large FOV microvascular image almost free of motion artifacts. But it is noted that there seem to be some artifacts (vertical or horizontal) still present, which are due to the imperfections caused by stitching the cubes together, not to the motion artifacts.

As is known, the NFL is formed by the expansion of the fibers of the optic nerve. Physiologically, the thickest part is located near the optic disk, gradually diminishing toward the *ora serrate*. The fiber bundles have an almost straight horizontal course and form an arch around the macula. The retinal vessels lie superficially to the nerve fiber bundles.[44] This feature of blood vessel appearance within the NFL is clearly observed on the OMAG angiogram (reddish color). The arch shaped region is located around the macula, while the change to an almost straight horizontal course takes place in the temporal region as shown in Fig. 5(a) (the red color). This is the first time that this feature is captured by OCT-based angiography, and the ability to provide imaging of such a vascular feature may be useful in the investigation of the retinal nerve fiber layer.

The magnified OMAG angiograms are selected to demonstrate the detail of blood vessels in different regions, including the optic nerve head [Fig. 5(b)], fovea [Fig. 5(c)], and temporal region [Fig. 5(d)]. The avascular region of the fovea is clearly seen in Fig. 3(c). In the temporal region, there are fewer dense fiber bundles and vessels [Fig. 5(d)].

To give a clear exhibition of the retinal vessel networks, we removed the NFL from the dataset and then displayed only the inner and outer retinal layers, as shown in Fig. 6(a). Red and green represent the inner and outer retinal layers, respectively. Excluding the NFL, the details of the retinal vessel can be appreciated. For comparison, the LSO image was also acquired and shown in Fig. 6(b). The magnified OMAG retinal angiogram is given in Fig. 6(c). A better visualization of the branches of the vascular tree is observed in the OMAG retinal angiogram compared to the LSO image. In addition, depth resolved capillary plexus can be clearly appreciated. The tacking LSO combined with OCT angiography provides better and much more precise images of the vasculature network of the retina than the existing clinical approaches. As is known, most eye diseases of the posterior segment, e.g., AMD and diabetic retinopathy, involve some changes to the vasculature. It is, therefore, expected that OMAG, performed with motion tracking, could be particularly useful in the diagnosis, treatment, and management of these eye diseases.

4 Conclusions and Discussion

We have demonstrated that OMAG is capable of providing high-fidelity and motion-free retinal microvascular images with the aid of real-time motion tracking. Motion tracking provides excellent repeatability and reliability over time when evaluating and quantifying the FAZ zone in macula. Such a feature is expected to be particularly useful in the accurate quantification of the longitudinal variations of FAZ for diagnosis and treatment monitoring of retinal diseases such as diabetic retinopathy. We have also shown that the motion tracking makes the montage scanning protocol feasible so that a large FOV of OMAG angiograms can be achieved, which would have a promising potential to extend the application of OCT-based angiography techniques.

In this paper, we leveraged the SLO motion tracking capability existing in the commercial Cirrus HD-OCT 5000 system to demonstrate the motion-free and ultrawide-field OMAG imaging of retinal microvasculature. With a relatively small eye movement (which is true for most of subjects), the system only took ~3.6 s to complete one OMAG cube scan. However, with severe eye movement, the system took substantially longer time to acquire a single volumetric data, which may reduce its utility in imaging relatively senior subjects whose eyes typically move rapidly. Fortunately, the system is equipped with a "locking-in" feature, meaning that the subject is allowed a rest and after a certain period of time, the machine automatically resumes the scanning at the position where it was interrupted as soon as the subject is repositioned in the system.

Another limitation of the current LSO motion tracking is that it does not track the motion in the z-direction. Thus, it would be expected that if there is z-motion, it would make the targeted retinal tissue out of focus, blurring the OMAG microvascular images, which on the other hand would affect our ability to quantify retinal microvascular parameters. One way to mitigate this problem is to use z software processing approach to compensate the z-motion by calculating the phase-shift between adjacent A-scans or B-Scan, representing the amount of tissue movement in the z-direction. However, such an approach would inevitably demand a heavy computational power, thus is not practical for clinical translation. Alternatively, we know that Doppler OCT is particularly useful in providing the real-time measurement of directional tissue movement in the z-axis.[45] Therefore, it would be expected that if Doppler OCT is incorporated into the motion tracking SLO mechanism, the z-motion artifacts can then be corrected to improve further the OMAG vascular imaging accuracy and fidelity, facilitating accurate quantification of retinal vessel parameters, e.g., flow index, vessel index, and tortuosity.[46]

Nevertheless, with continued improvement of the motion-tracking system, it is expected that the combination of real-time motion tracking with OCT angiography will provide a viable clinical tool for more precise and accurate visualization and quantification retinal vascular network in the aid of early diagnosis, therapeutic treatment, and management of the eye diseases that have vascular involvement.

Acknowledgments

This work was supported in part by research grants from the Carl Zeiss Meditec, Inc. (Dublin, California), the National Eye Institute (R01EY024158), an unrestricted grant from Research to Prevent Blindness, and the Department of Bioengineering at the University of Washington. The content is solely the responsibility of the authors and does not necessarily represent the official views of the grant-giving bodies.

References

1. D. Huang et al., "Optical coherence tomography," *Science* **254**(5035), 1178–1181 (1991).
2. P. H. Tomolins and R. K. Wang, "Theory, developments and applications of optical coherence tomography," *J. Phys. D Appl. Phys.* **38**(15), 2519–2535 (2005).
3. W. Drexler and J. G. Fujimoto, "State-of-the-art retinal optical coherence tomography," *Prog. Retinal Eye Res.* **27**(1), 45–88 (2008).
4. A. F. Fercher et al., "Measurement of intraocular distances by backscattering spectral interferometry," *Opt. Commun.* **117**(1–2), 43–48 (1995).
5. M. Wojtkowski et al., "Ultrahigh-resolution, high-speed, Fourier domain optical coherence tomography and methods for dispersion compensation," *Opt. Express* **12**(11), 2404–2422 (2004).
6. R. K. Wang et al., "Three dimensional optical angiography," *Opt. Express* **15**, 4083–4097 (2007).
7. R. K. K. Wang, "Optical microangiography: a label-free 3-D imaging technology to visualize and quantify blood circulations within tissue beds *in vivo*," *IEEE J. Sel. Top. Quantum Electron.* **16**, 545–554 (2010).
8. Z. Chen et al., "Optical Doppler tomographic imaging of fluid flow velocity in highly scattering media," *Opt. Lett.* **22**(1), 64–66 (1977).
9. L. An, T. T. Shen, and R. K. K. Wang, "Using ultrahigh sensitive optical microangiography to achieve comprehensive depth resolved microvasculature mapping for human retina," *J. Biomed. Opt.* **16**(10), 106013 (2011).
10. R. K. Wang et al., "Depth-resolved imaging of capillary networks in retina and choroid using ultrahigh sensitive optical microangiography," *Opt. Lett.* **35**, 1467–1469 (2010).
11. R. K. Wang et al., "Feasibility to image retinal microvasculature in subjects with diabetic retinopathy using Zeiss Cirrus OCT prototype system," *Invest. Ophtal. Visual Sci.* **55**(5), 216 (2014).
12. M. R. Thorell et al., "Swept-source OCT angiography of macular telangiectasia type 2," *Ophthalmic Surg. Lasers Imaging Retina* **45**(5), 369–380 (2014).
13. S. Martinez-Conde, S. L. Macknik, and D. H. Hubel, "The role of fixational eye movements in visual perception," *Nat. Rev. Neurosci.* **5**(3), 229–240 (2004).
14. T. Klein et al., "Megahertz OCT for ultrawide-field retinal imaging with a 1050 nm Fourier domain mode-locked laser," *Opt. Express* **19**(4), 3044–3062 (2011).
15. B. Potsaid et al., "Ultrahigh speed spectral/Fourier domain OCT ophthalmic imaging at 70,000 to 312,500 axial scans per second," *Opt. Express* **16**(19), 15149–15169 (2008).
16. S. Ricco et al., "Correcting motion artifacts in retinal spectral domain optical coherence tomography via image registration," *Med. Image Comput. Comput. Assisted Intervention* **12**(1), 100–107 (2009).
17. M. F. Kraus et al., "Motion correction in optical coherence tomography volumes on a per A-scan basis using orthogonal scan patterns," *Biomed. Opt. Express* **3**(6), 1182–1199 (2012).
18. K. V. Vienola et al., "Real-time eye motion compensation for OCT imaging with tracking SLO," *Biomed. Opt. Express* **3**(11), 2950–2963 (2012).
19. B. Braaf et al., "Real-time eye motion correction in phase-resolved OCT angiography with tracking SLO," *Biomed. Opt. Express* **4**(1), 51–65 (2013).
20. D. A. Robinson, "A method of measuring eye movement using a scleral search coil in a magnetic field," *IEEE Trans. Biomed. Eng.* **10**(4), 137–145 (1963).
21. H. D. Crane and C. M. Steele, "Generation-V dual-Purkinje-image eye-tracker," *Appl. Opt.* **24**(4), 527–537 (1985).
22. T. N. Cornsweet and H. D. Crane, "Accurate two-dimensional eye tracker using first and fourth Purkinje images," *J. Opt. Soc. Am.* **63**(8), 921–928 (1973).
23. R. W. Ditchburn and B. L. Ginsborg, "Involuntary eye movements during fixation," *J. Physiol.* **119**(1), 1–17 (1953).
24. T. N. Cornsweet, "New technique for the measurement of small eye movements," *J. Opt. Soc. Am.* **48**(11), 808–811 (1958).
25. R. H. Webb and G. W. Hughes, "Scanning laser ophthalmoscope," *IEEE Trans. Biomed. Eng.* **BME-28**(7), 488–492 (1981).

26. R. H. Webb, G. W. Hughes, and F. C. Delori, "Confocal scanning laser ophthalmoscope," *Appl. Opt.* **26**(8), 1492–1499 (1987).
27. J. B. Mulligan, "Recovery of motion parameters from distortions in scanned images," in *Proc. NASA Image Registration Workshop (IRW 97)*, pp. 281–292, NASA Goddard Space Flight Center, Maryland (1997).
28. M. Stetter, R. A. Sendtner, and G. T. Timberlake, "A novel method for measuring saccade profiles using the scanning laser ophthalmoscope," *Vision Res.* **36**(13), 1987–1994 (1996).
29. D. P. Wornson, G. W. Hughes, and R. H. Webb, "Fundus tracking with the scanning laser ophthalmoscope," *Appl. Opt.* **26**(8), 1500–1504 (1987).
30. R. D. Ferguson et al., "Tracking optical coherence tomography," *Opt. Lett.* **29**(18), 2139–2141 (2004).
31. D. Hammer et al., "Advanced scanning methods with tracking optical coherence tomography," *Opt. Express* **13**(20), 7937–7947 (2005).
32. R. Ferguson et al., "Wide-field retinal hemodynamic imaging with the tracking scanning laser ophthalmoscope," *Opt. Express* **12**(21), 5198–5208 (2004).
33. D. X. Hammer et al., "Angiography with a multifunctional line scanning ophthalmoscope," *J. Biomed. Opt.* **17**(2), 026008 (2012).
34. Y. P. Huang et al., "Swept-source OCT angiography of the retinal vasculature using intensity differentiation based OMAG algorithms," *OSLI Retina* **45**(5), 382–389 (2014).
35. U. Sharma and M. Everett, "Data acquisition methods for reduced motion artifacts and applications in OCT angiography," U.S. Patent 8,857,988.
36. http://www.zeiss.com.
37. L. An, T. T. Shen, and R. K. K. Wang, "Using ultrahigh sensitive optical microangiography to achieve comprehensive depth resolved microvasculature mapping for human retina," *J. Biomed. Opt.* **16**(10), 106013 (2011).
38. L. An et al., "High-resolution wide-field imaging of retinal and choroidal blood perfusion with optical microangiography," *J. Biomed. Opt.* **15**(2), 026011 (2010).
39. X. Yin, J. R. Chao, and R. K. Wang, "User-guided segmentation for volumetric retinal optical coherence tomography images," *J. Biomed. Opt.* **19**(8), 086020 (2014).
40. S. Zotter et al., "Visualization of microvasculature by dual-beam phase-resolved Doppler optical coherence tomography," *Opt. Express* **19**(2), 1217–1227 (2011).
41. B. Braaf et al., "Angiography of the retina and the choroid with phase-resolved OCT using interval-optimized backstitched B-scans," *Opt. Express* **20**(18), 20516–20534 (2012).
42. J. Hu et al., "Improved repeatability of retinal thickness measurements using LSO image-based tracking," *Invest. Ophthalmol. Visual Sci.* **54**, 3621 (2013).
43. H. C. Hendargo et al., "Auomated non-rigid registration and mosaicing for robust imaging of distinct retinal capillary beds using speckle variance optical coherence tomography," *Biomed. Opt. Express* **4**(6), 803–821 (2013).
44. R. L. Radius and J. de Bruin, "Anatomy of the retinal nerve fiber layer," *Invest. Ophthalmol. Visual Sci.* **21**(5), 745–749 (1981).
45. R. K. Wang, Z. Ma, and S. J. Kirkpatrick, "Tissue Doppler optical coherence elastography for real time strain rate and strain mapping of soft tissue," *Appl. Phys. Lett.* **89**, 144103 (2006).
46. R. Reif et al., "Quantifying optical microangiography images obtained from a spectral domain optical coherence tomography system," *Int. J. Biomed. Imaging* **2012**, 509783 (2012).

Biographies for the authors are not available.